THE CORRECTION OF INFRASOUND SIGNALS FOR UPPER ATMOSPHERIC WINDS

J. Paul Mutschlecner and Rodney W. Whitaker
Los Alamos National Laboratory

INTRODUCTION

Infrasound waves propagate in the atmosphere by a well known mechanism produced by refraction of the waves, return to earth, and reflect at the surface into the atmosphere for subsequent bounces (see e.g. reference 1). Figure 1 illustrates this phenomenon with results from a ray trace model. In this instance three rays are returned to earth from a region centered at about 50 kilometers in altitude and two from a region near 110 kilometers in altitude. The control of the wave refraction is largely dominated by the temperature-height profile and inversions; however, a major influence is also produced by the atmospheric wind profile. Figure 2 illustrates the considerable ray differences for rays moving in the wind direction (to the right) and in the counter direction (to the left). It obviously can be expected that infrasonic signal amplitudes will be greatly influenced by the winds in the atmosphere. The seasonal variation of the high altitude atmospheric winds is well documented (see e.g. reference 2). Figure 3 illustrates this with average statistics on the observed zonal wind in the region of 50 ± 5 kilometers in altitude. The results are based upon a survey by Webb (reference 2); Webb terms this parameterization the Stratospheric Circulation Index (SCI). The very strong seasonal variation has the ability to exert a major seasonal influence on infrasonic signals. It is our purpose to obtain a method for the correction of this effect.

METHODOLOGY

There are two possible approaches to the determination of a procedure for the correction of infrasound signals for the effects of winds. The first of these is by modeling of infrasonic propagation in the presence of various wind profiles. We are currently taking this approach with both a ray-trace model and a normal mode model and hope to show results in the near future. The second approach is to derive a correction method empirically from a sufficiently large and consistent data set. This is the method which we report upon here. The results given here are preliminary in nature and we present only a simplified outline of the procedures. As indicated in Section IV, more extensive work in the near future will provide comprehensive results. In the meantime, we have been applying the results to our measurements (see reference 3).

A large data set, which appears to be appropriate for the empirical work, is given in reference 4. It consists of infrasonic observations by the Sandia National Laboratory of atmospheric nuclear tests conducted at the Nevada Test Site (NTS) during the period 1951 to 1962. The observations were made at nine stations surrounding NTS as shown in figure 4. While several of the stations are probably too close to the source region to be useful, at least six stations appear to be appropriate. A total of 80 events are presented by Reed and cover an explosive yield range from 1/2 to 74 kilotons (HE equivalent). The measurements were made by a standard set of microbarographs.

This consistently measured and analyzed set of signals, observed at many times of the year, presents a unique set of data for our purposes.

ANALYSIS AND RESULTS

Since the atmospheric nuclear data are for a variety of yields, and also have effects due to some variation in height of burst, it is necessary to scale all data for these two factors. Reed has done this with a $W^{0.4}$ scaling law (W = kilotons HE equivalent) and a height-of-burst functional relation. While some discussion of both of these scaling relations is appropriate, the preliminary nature of the present work leads to use of Reed's corrections.

Figure 5 illustrates the resulting scaled data for the St. George, Utah, station as a function of date. The symbols refer to various test series, unimportant here, and the line is an eye-fitted relation. Amplitudes are scaled to a 1 kiloton explosion. The very strong seasonal effect is the major feature of the data; the much lower amplitude during the summer period presumably results from the winds contrary to wave propagation to St. George during summer. It is unfortunate that there are no data for the period in mid winter, January - December. Examination of Reed's results shows that the seasonal variation changes markedly with station direction from the test site: northern and southern stations show a much weaker effect than does St. George. This follows from the fact that those stations are only slightly affected by the zonal wind and are primary affected by the much weaker and less variable meridional winds. This supports the hypothesis that we see primarily the seasonal wind effect in the data variation.

High altitude winds are conventionally measured by rocketsonde (and now by satellite). The absence of rocketsonde observations for the period covered by the NTS data leads us to use the statistical SCI data of reference 2 as a first-order estimator of the atmospheric wind. The eye-fitted lines for each station (e.g. figure 5) were used to estimate signal amplitudes at monthly intervals. Figure 6 illustrates the result for St. George, where the wind

144

velocity component directed from NTS to St. George is plotted against the amplitude. Similar relations are determined for each station, using the wind vector toward the station based upon meridional and zonal SCI values. The results are reasonably consistent among the stations; however, the nearly east or west stations, such as St. George, are probably more dependable because of the strong zonal wind variation there.

The averaged result of the analysis is,

$$A = A_0 \, 10^{kV}$$

where

A = observed amplitude (mbars)

A_0 = corrected "zero-wind" amplitude (mb)

k = 0.018 s/meter

V = SCI vector from source to observer meters/s.

The relation permits us to correct all observations for the wind to derive consistent "zero-wind" amplitudes.

COMMENTARY ON RESULTS

We have applied the method described here to a wide variety of observations. Where possible, we have used rocketsonde or satellite observations of the wind profile, deriving from these an effective SCI wind vector amplitude. Since the actual wind can vary widely from the statistical SCI, use of statistical values is less dependable. As an example of the use of the method, we show its application to a set of observations of signals from a set of earthquakes which were observed at our St. George array, with the exception of the earthquake at M_b = 7.8, which is from reference 5. All amplitudes have been scaled to a distance of 1000 kilometers by use of the factor $(R/1000)^{1.15}$, where R is the actual range in kilometers. Figure 7 shows the amplitudes <u>uncorrected</u> for wind against the body magnitude, M_b, for each earthquake. The bars on some observations indicate the range of interpretation of peak amplitude. Figure 8 shows the same set of data but with the amplitudes <u>corrected</u> by our method; only statistical SCI winds were employed. Clearly the effect on the relationship is very large; there is also the impression that the connection between amplitude and M_b may be

clearer. However, a mechanism is not now known, so this evidence is circumstantial. The smallest earthquake, at $Mb = 4.6$, is an aftershock and may not be in the same class as the others.

We have not completed our analysis of the nature of the wind effect on amplitudes and therefore can only speculate on the correction method and its form. It is clear that two mechanisms can change the amplitude with change in the wind profile: (1) the number of rays captured at a return layer will vary depending upon the wind, (2) the distribution of rays on the surface will depend on the wind profile (e.g., see figure 2). Modeling should help in the understanding of the correction form.

It should be noted that all of the work reported here applies to those signals resulting from returns from a 50 kilometer high level. We believe that signals resulting from the 110 kilometer level require an additional correction and have formulated a tentative correction formulation. Such signals, in general, will occur only with near zero wind, or counterwind, conditions.

FUTURE EFFORTS

We have reported here on our preliminary results. We are now working on an improved analysis. This will include the following:

1.   A comprehensive statistical analysis of the data set resulting in an improved formulation;

2.   Modeling of the effect to better understand its physical basis;

3.   A detailed investigation of the "counterwind" signal circumstances, using appropriate data and modeling.

REFERENCES

1. Gossard, Earl E.; Hooke, William H.: Waves in the Atmosphere. Elsevier Sci. Pub. Co., 1975, Ch. 9.

2. Webb, Willis L: Structure of the Stratosphere and Mesosphere. Academic Press, 1966.

3. Whitaker, Rodney W.; Mutschlecner, J. Paul; and Davidson, Masha B.: Infrasonic Observations of Large Scale HE Events. Fourth International Symposium on Long Range Sound Propagation, NASA CP-3101, 1990.

4. Reed, Jack W.: Climatology of Airblast Propagation from Nevada Test Site Nuclear Airbursts. Sandia Laboratories Research Report, SC-RR-69-572, 1969.

5. Young, Jessie M.; and Greene, Gary E.: Anomalous Infrasound Generated by the Alaskan Earthquake of March 28, 1964. J. Acoust. Soc. of Am., 71 (2), February 1982.
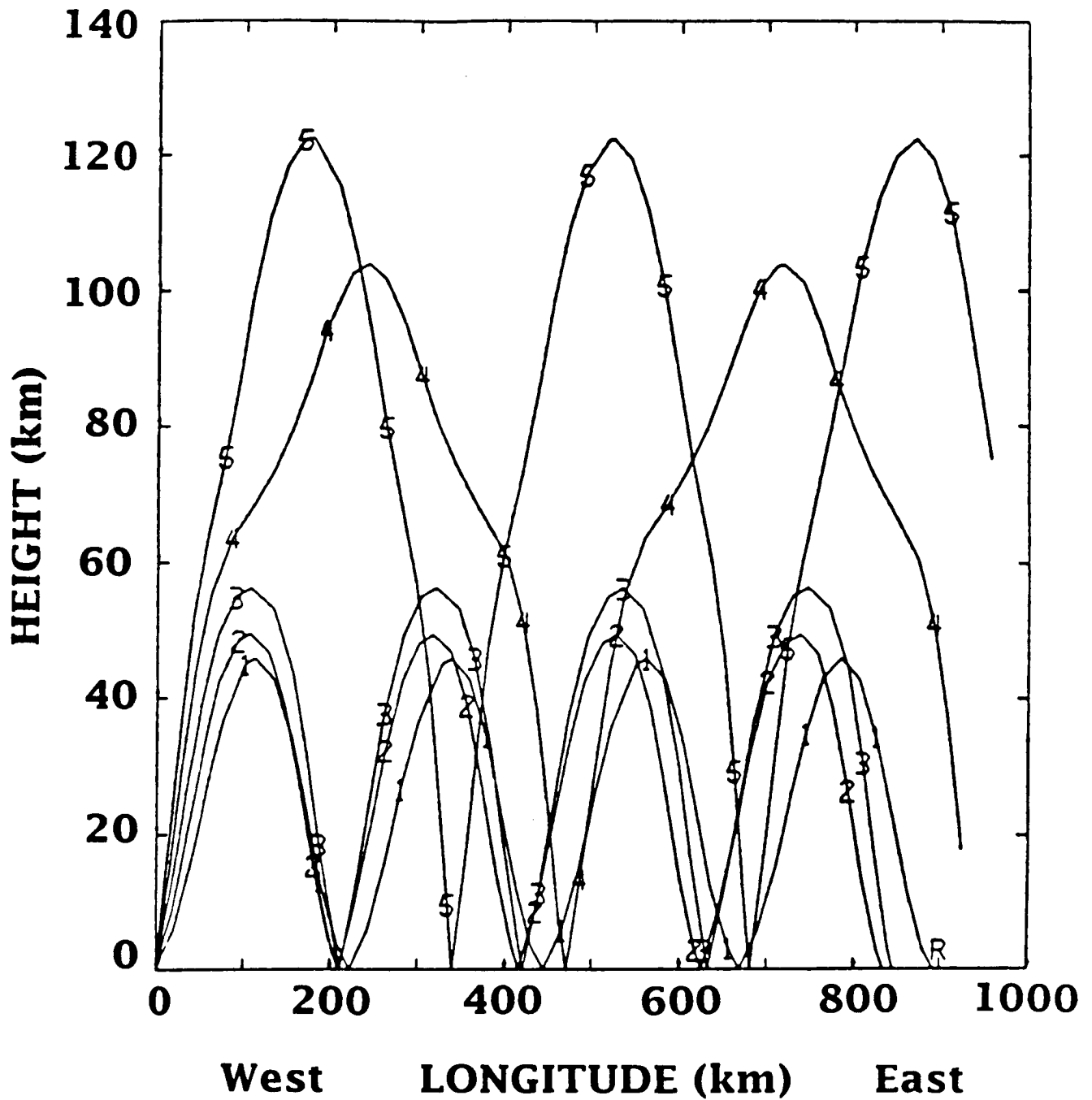
Figure 1. Results of a ray trace model showing five sample rays. Rays 1, 2, 3 are refracted and returned from a region near 50 kilometers and rays 4 and 5 from near 110 kilometers.
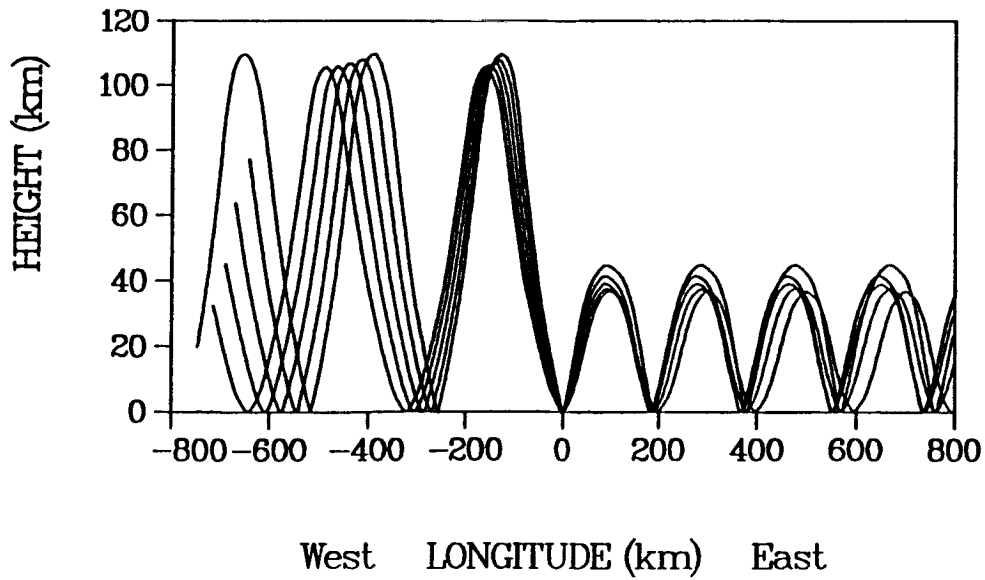
Figure 2. Ray tracing results for propagation with the wind (to the right) and against the wind (to the left).

SEASONAL VARIATION OF MEAN S.C.I.
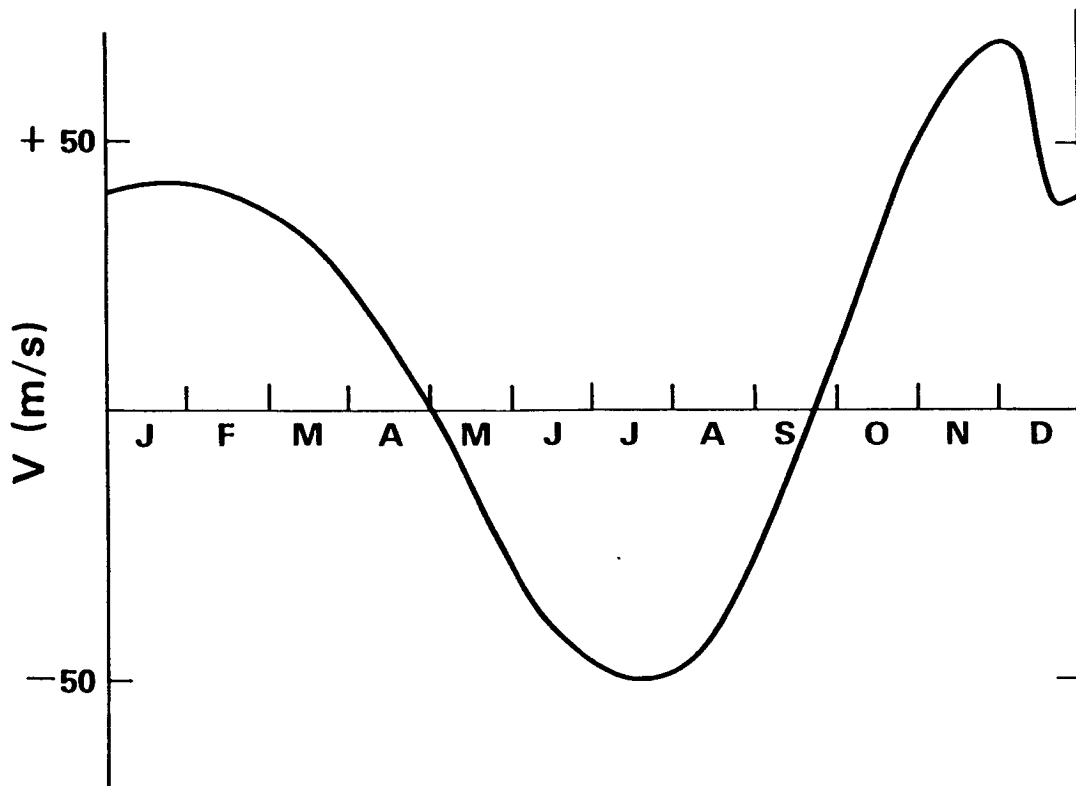
Figure 3. This illustrates the seasonal variation of the average SCI wind at White Sands.

Sandia Network
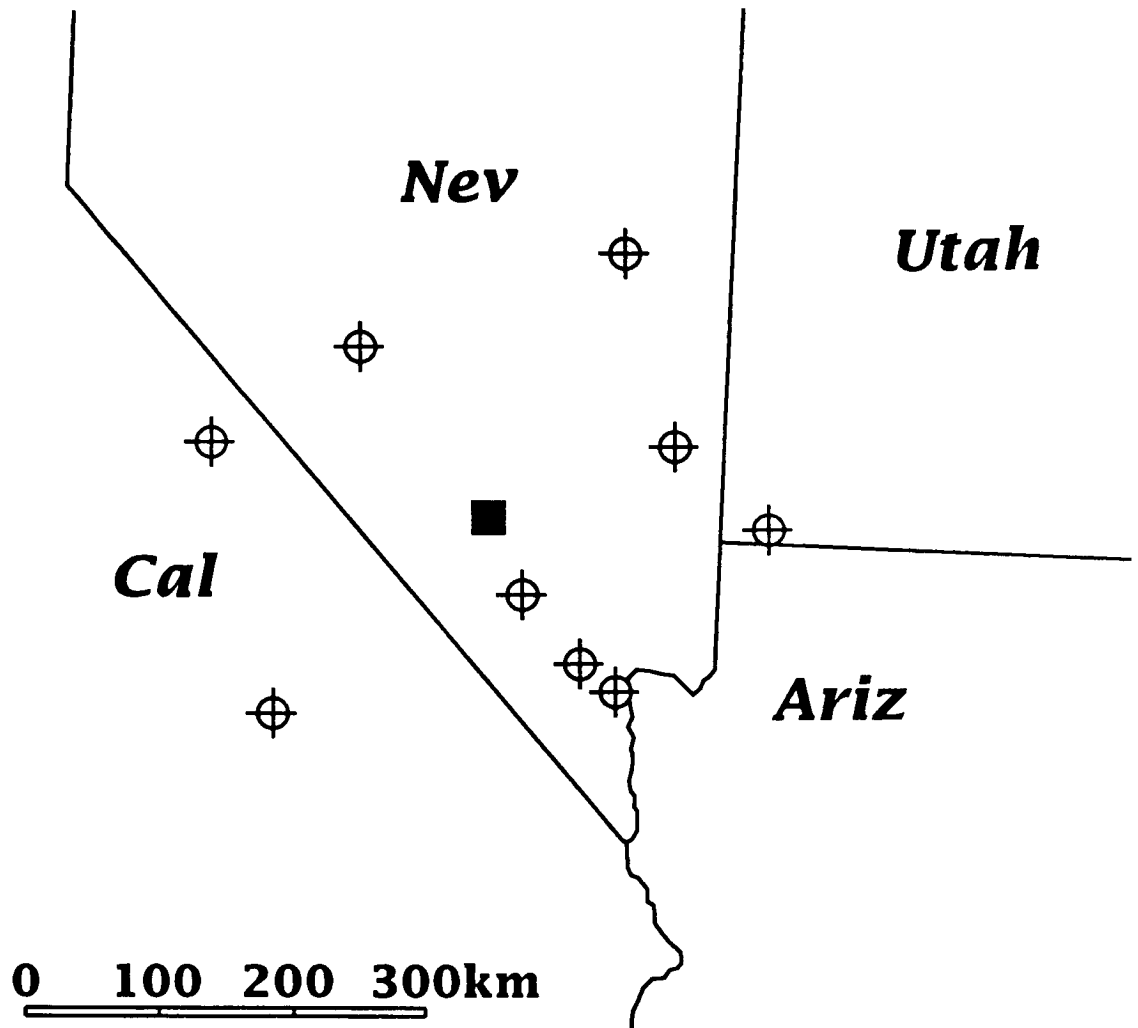
Figure 4. The Sandia Scientific Laboratory network of microbarographs (crossed circles) surrounding the Nevada Test Site (square).
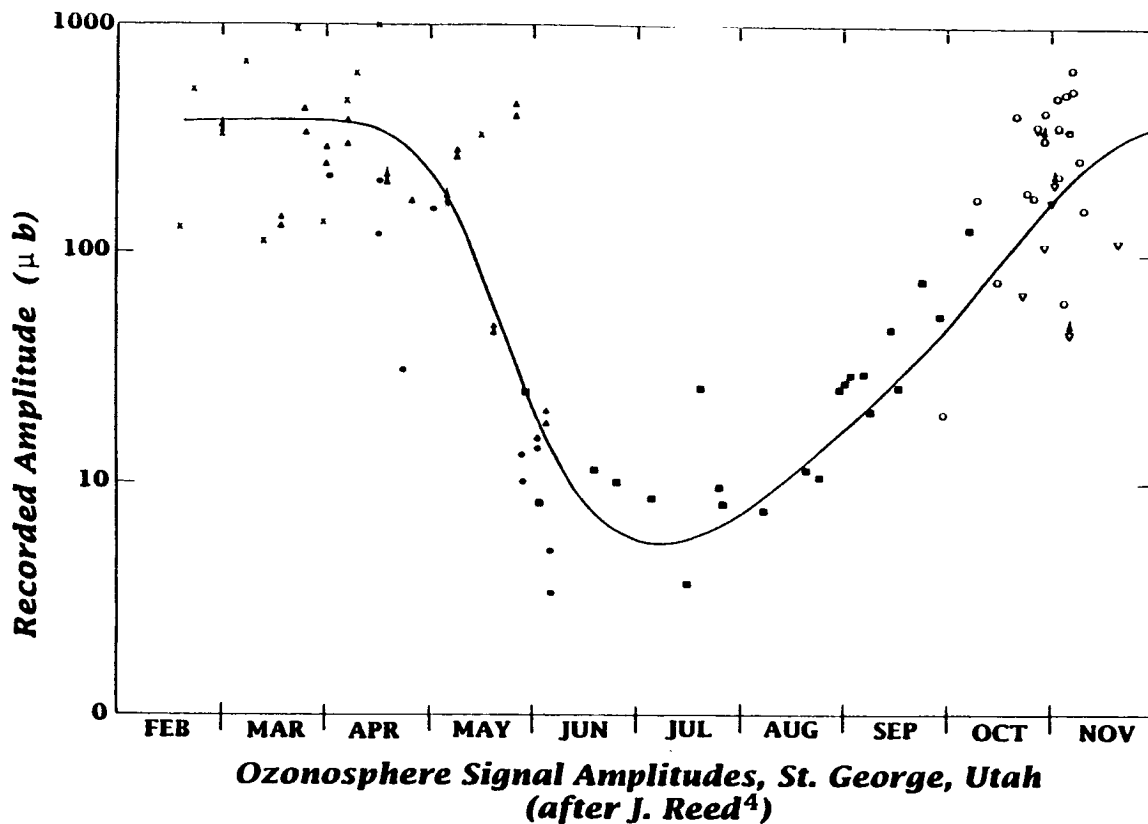
Figure 5. Nuclear atmospheric burst scaled signal amplitudes recorded at the St. George, Utah, microbarograph station against date.
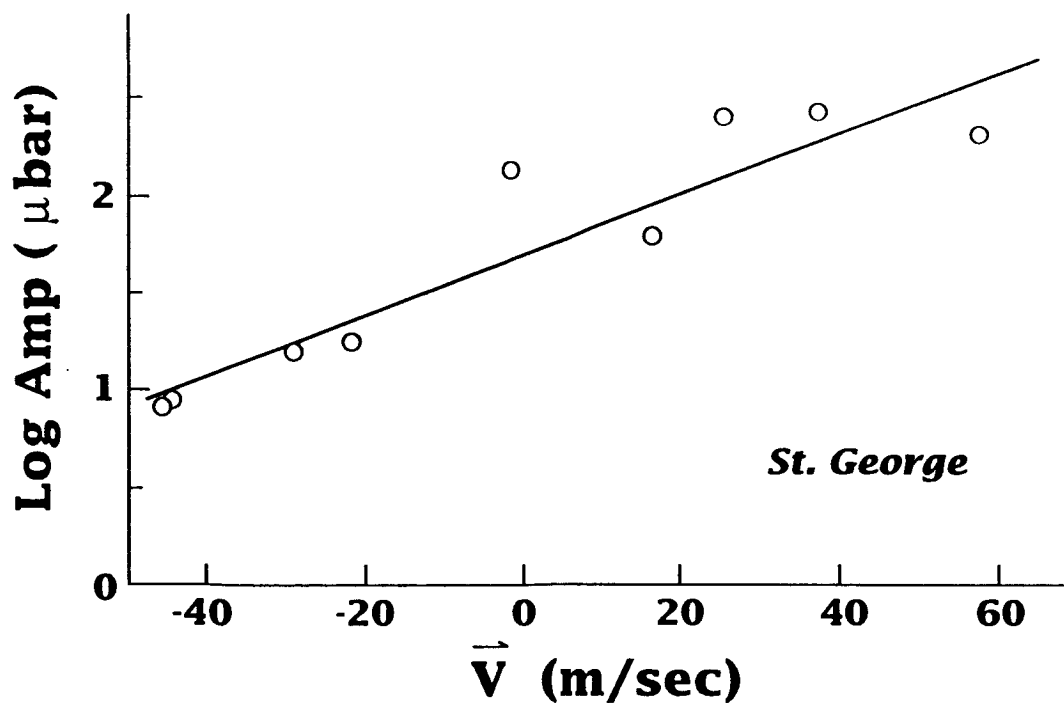

Figure 6. Monthly average values of nuclear atmospheric burst scaled signal amplitude versus statistical SCI velocity for St. George.
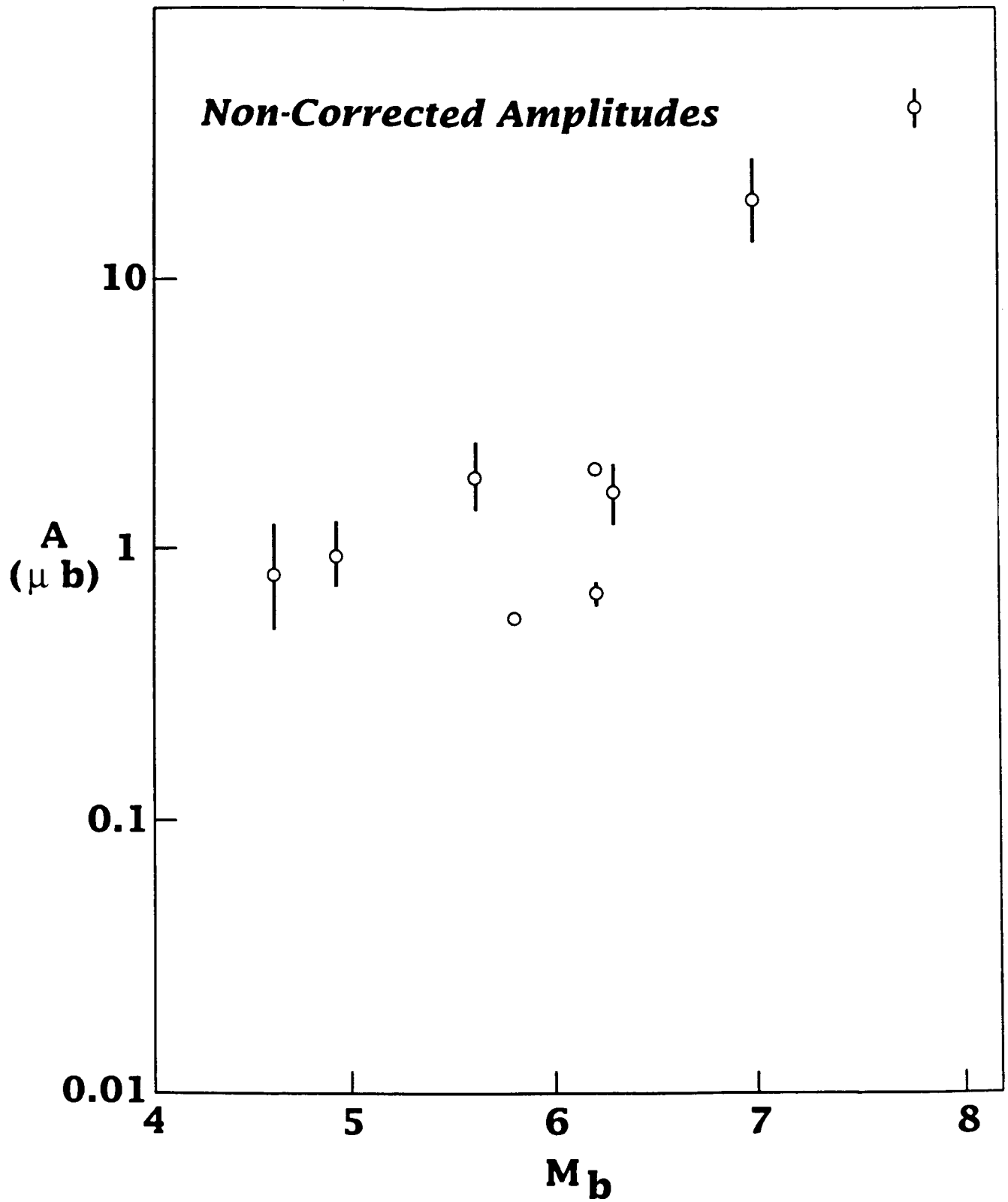
Figure 7. Scaled amplitudes of earthquake infrasonic signals versus earthquake body magnitude, M_b. Uncorrected for wind.
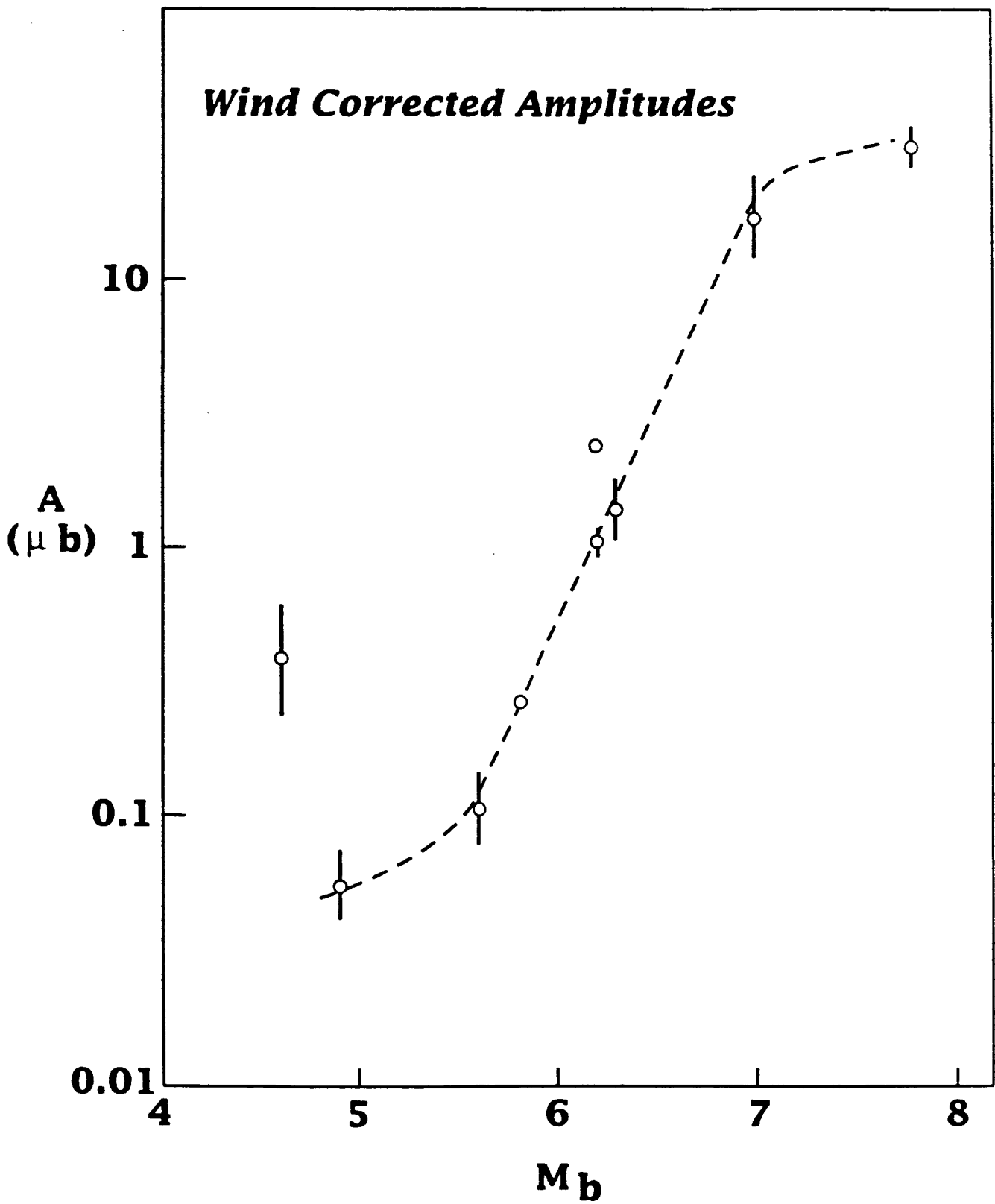
Figure 8. Same data as in Figure 7, but corrected for wind.